Review

Finite Element Models to Predict the Risk of Aseptic Loosening in Cementless Femoral Stems: A Literature Review

Xiaoshu Sun [1] , Cristina Curreli [2,*] and Marco Viceconti [1,2]

1   Department of Industrial Engineering, Alma Mater Studiorum, University of Bologna, 40126 Bologna, Italy;
    xiaoshu.sun@unibo.it (X.S.); marco.viceconti@unibo.it (M.V.)
2   Medical Technology Lab, IRCCS Istituto Ortopedico Rizzoli, 40136 Bologna, Italy
*   Correspondence: cristina.curreli@ior.it; Tel.: +39-051-636-6564

Abstract: Aseptic loosening is the most common failure mode for total hip arthroplasty, and the design of the implant plays a significant role in influencing the longevity and stability of the implant. Finite Element (FE) models have been demonstrated to be powerful numerical tools that allow for generating information supporting the device's safety and/or efficacy during pre-clinical assessment. Different authors have proposed FE studies aiming to simulate the long-term stability of the femoral stem; however, multiple improvements are still necessary for translating computational methodologies into clinical practice. This paper provides a comprehensive overview of the modelling procedures for predicting aseptic loosening risk, focusing on cementless femoral stems. The main modelling assumptions, including bone and implant geometry, materials, boundary conditions, and bone–implant interface contact, were summarised and presented. The limitations of various modelling assumptions and their impact on the simulation results were also discussed. The analysis suggests that more rigorous clinical validation for osseointegration models and failure criteria used to determine loosening of the implant should be clearly defined, and efforts should be made to identify the appropriate limit of tolerable conditions.

1. Introduction

Since the 1960s, total hip arthroplasty (THA) has proven to be successful in alleviating hip pain, enhancing mobility and quality of life, and enabling patients to resume regular activities. Over three million primary THAs are performed annually in Europe [1,2], and different studies suggest that a further increase in demand is anticipated over the next 20 years [3,4]. From an engineering point of view, THAs can be mainly classified as cemented or cementless, depending on the implant fixation modality. Cementless fixation, which relies on press fit and osseous integration, has gained popularity over the past decade, both for cups and stems [5,6]. According to the latest report on primary THAs from the Register of the Orthopaedic Prosthetic Implants register, between 2017 and 2019, cementless cups and stems accounted for 99% and 96.7% of all operations, respectively, in Italy [7]. The latest National Joint Registry annual report also indicates a total number of primary uncemented hip replacements higher than that of cemented implants [8].

Despite being one of the most effective and commonly performed orthopaedic procedures, with a 10-year survival rate of over 90% shown in cementless implants [5], the number of implant revisions is continuously rising, mainly due to the growing number of primary surgeries. Given the significant medical and economic burden associated with the revision surgery, the significance of paying closer attention to THA failure and lowering the risk is self-evident. The THA failure patterns frequently observed include aseptic loosening (AL), infection, periprosthetic fracture, and instability. Aseptic loosening remains

the leading cause of failure, as evident in most hip replacement registers. The reported values for the AL failure incidence range from 40% to 70% [9–11].

Aseptic loosening is described as the failure of the bone–implant fixation in the absence of infection [12]. Although AL can occur due to inadequate initial fixation (e.g., small-to-fit), it is primarily associated with mid- and long-term instability rather than a lack of primary stability. While substantial evidence has been observed regarding the mechanics of AL, it is difficult to attribute it to a single cause. Aseptic loosening is often accompanied by periprosthetic osteolysis, which refers to bone resorption around the implant as well as an inflammatory cellular response within the joint. Additionally, excessive micromotion at the bone–implant interface or the abrasion of polyethene particles from wear can also contribute to AL [12]. More practically speaking, AL is caused by various preoperative, intraoperative, and post-operative factors, including patients' bone quality, implant properties, surgical technique, and lifestyles. Among them, the implant designs play a crucial role in the procedure's success [13]. Clinical studies conducted long-term follow-up assessments to track the survival rate of THAs with various implant types, with some highlighting the AL rate of cementless femoral implants. In many cementless stem designs, a 10-year survivorship rate of over 96% has been observed (e.g., ABG I, Osteonics Cementless, R-B Interlok, Zweymuller-Alloclassic, Freeman Cementless) [14]. At 4.5 years, the estimated probability of revision for AL was 18.6% for the Bio-Fit stem (cobalt-chromium; straight stem) and 0.5% for the Corail stem (Titanium; straight stem) [15]. Another 5-year follow-up study conducted on 517 cementless THAs found an unusually high number of AL failure cases after using a modified stem with a shorter and shoulder-less double-taper [16]. The revision rate for the smaller Corail stem was four times higher than that for larger femoral diameters [17]. Different implant designs show a considerably different incidence of AL, which confirms that implant design is a major determinant.

Therefore, studying the effect of various femoral implant types on failure risk is crucial for improving patient safety, reducing costs, and improving long-term outcomes. Conventional methods for predicting the AL failure risk and assessing the safety of the implant devices preoperatively include in vitro experiments, animal experiments, and clinical trials. However, each approach has its limitations. One notable weakness of in vitro experiments is their inability to fully replicate the conditions of cells or tissues in a living organism [18]. Animal experiments can maintain biological conditions, but they may not be equivalent to clinical conditions in human patients [19]. Clinical trials are time consuming, costly, and limited in this long-term failure risk investigation. One promising alternative to traditional methods is represented by the use of computer modelling and simulation. In particular, Finite Element (FE) modelling, has been demonstrated to be a powerful numerical tool that allows for generating information supporting the device's safety and/or efficacy. It holds promise for assessing whether subtle modifications in orthopaedic devices can enhance existing designs while accounting for patient and surgical variability [20–22]. A virtual cohort of simulated patients can be used to optimise implant design, including material selection, geometry, and surface features (In Silico Trials) [23,24]. Also, with patient-specific models, surgeons can create a virtual replica of a patient's anatomy (Digital Twins), personalise the planning, and optimise the surgical outcome [25].

A large body of literature has used FE modelling to investigate the biomechanical interaction between bone and cementless femoral implants in the context of AL failure. This literature covers a broad range of topics and can be categorised into subsets based on the various aspects related to AL that have been specifically analysed. Some researchers simulated the complex interactions between the implant and surrounding bone by quantifying parameters such as stress distributions, micromotion, osseo-integrated area, and bone remodelling [26–32]. Most of the studies focused on mitigating the risks of AL from various perspectives. For instance, some have evaluated the mechanical performance of stems with different parameters, such as geometric features and materials [27,28,30–39]. Others have examined the effect of bone quality [40,41], surgical variability, and patients lifestyles [29,32,34,41,42] on the risk of failure. While some articles have attempted to

review the literature on numerical simulation of orthopaedic devices [21,43], including in some cases analyses on post-operative bone growth and long-term bone adaptation [44], to the best of the authors' knowledge, none provide a comprehensive overview of the use of FE simulations to specifically investigate AL failure risk in cementless femoral stems.

The aim of this paper is to address this gap by providing a comprehensive overview of the main modelling procedures for predicting AL risk in cementless femoral stems due to a lack of long-term stability. The review will assess papers based on several criteria, including bone and implant geometry modelling, loading patterns considered, contact models, and output quantities analysed. For most of these criteria, the main limitations and effects of the different modelling assumptions on the simulation results will also be discussed.

2. Studies Selection

By conducting a comprehensive search of the PubMed databases, an initial list of relevant publications was generated using the key terms: ((hip replacement) OR (hip arthroplasty) OR (hip implant)) AND ((Finite Element) OR (simulation) OR (modelling)) AND ((aseptic loosening) OR (bone remodelling) OR (bone ingrowth) OR (osseointegration)). One important point to note is that when conducting a literature search on the prediction of AL failure modes using FE modelling, some researchers use terms such as 'bone ingrowth', 'bone remodelling', and 'osseointegration' instead of directly referring to AL or long-term stability failure of the implant. This variation in indirect terminology can be attributed to the multifactorial nature of AL. It is therefore advisable to consider these indirect searches to ensure a more comprehensive coverage of the literature.

Potentially eligible articles were initially screened by title and abstract. If they did not match any of the following categories, they were excluded:

- hip joint replacement;
- Finite Element models;
- failure modes related to aseptic loosening.

After a thorough reading of the full manuscripts, studies were further excluded if they met any of the following criteria:

- osseointegration at the bone implant interface was not modelled;
- the implants were cemented;
- only lack of primary stability was simulated.

To clarify the last exclusion criterion, it is important to note that there is a significant body of literature that focuses on the mechanical behaviour of primary stability, which is an important risk factor for the AL of cementless hip implants. And evidence was found that early peri-implant bone healing immediately after implantation and the consequent mechanical remodelling at the bone–implant interface are essential for secondary implant stability [45,46]. However, it is the secondary stability that directly leads to the occurrence of AL. Hence, if the study only investigated primary stability without any consideration of long-term adaptative biological evolution, it was excluded from this review. It should also be noted that conference proceedings were excluded from the analysis, and only research journal articles published in the last three decades (1994-today) were considered. Of the 946 papers that our initial search identified, at the end of this selection process, by removing the overlap and based on the criteria above, 22 papers were considered for this review. This final selection also includes six additional sources that were identified after examining the bibliography of all relevant articles. The flowchart of article selection is depicted in Figure 1. The studies will be detailed in the following sections according to suitable model assumptions for the following aspects:

a.   characteristics of bone and implant modelling (e.g., geometry, surgical pose, material properties, and meshing);
b.   boundary conditions;
c.   bone–implant interface contact;
d.   quantities of interest used to predict the failure mode.
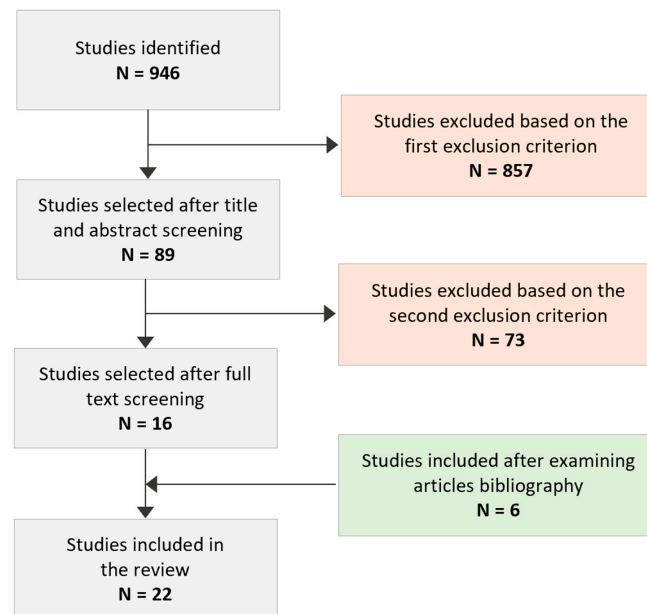
Figure 1. Flowchart of article selection.

3. Search Results

3.1. Bone and Implant Features

3.1.1. Geometry

Bone

Most 3D FE models have been developed by directly segmenting the bone geometry from computed tomography (CT) scan datasets of the patients and reducing the length of the original femur by resecting the distal part of the bone to reduce the computational cost (Table 1). Medical image processing software such as MIMICS® (Materialise, Leuven, Belgium) was typically used in most of the selected works to process CT scan data and distinguish bone from soft tissue using CT number threshold values [28,34]. In some cases, the three dimensional geometry of a composite femur was used as a standard reference for the FE model (Table 1) [26,29–32]. Instead of the intact bone–implant model, few studies solely mimic the local adjacent region of bone–implant interfaces based on a cubic 3D CAD model [36,39,47] or a plane 2D model [48]. In addition, simplified cylindrical 3D models were reconstructed in [33,40].

Implant

As shown in Table 1, only a few studies used simplified cylindrical or truncated cone shapes to model the femoral stem implant [33,49], while cubic and planar geometries were considered only for local models that include the adjacent regions of the bone–implant interface [36,39,47]. The majority of FE models of the implant were derived from commercial stem designs. Implants with different outline structures and surface morphologies have been tested as comparative characteristics to investigate whether implant geometries affect stability [27,28,30,32,34–36,39,50]. For example, S. Chanda et al. investigated osseointegration and bone remodelling performance using two fully coated cementless hip stems, one obtained from a generic TriLock (DePuy, USA) design and the other derived from a shape optimisation study [27]. J. Folgado et al. [30] compared two commercial stems: the tapered stem (Trilock by DePuy) and a cylindrical cross-sectioned stem (AML by DePuy). The tapered stem was found to be intrinsically more stable than the cylindrical stem with a similar fit and material. P.K. Puthumanapully et al. [35] focused on the short-stemmed implants and found that more bone formation occurred in the short stem with the lateral flare present compared to when the flare was absent.

Few studies have demonstrated that the implant surface texture might significantly improve bone ingrowth, while non-textured implants might promote fibrous tissue forma-

tion [34,36,39]. Specifically, three types of stem surface macro-textures were compared in [36,44]: softer connective tissues and relatively less bone growth were observed at the edges of the grooves/ribs, where high-stress concentration occurs. In addition, some authors simulated the coating surface based on a porous microstructure [33,48,51]. F. Tarlochan et al. [33] compared the functionally graded porous with two diameters of homogenous porous microstructures on implant stability. Models with larger pore sizes predicted fewer chances of bone ingrowth, and functionally graded porous surfaces promoted stability and reduced the failure chance.

A few implant shape optimisation studies were also conducted in [27,32]. R.B. Ruben et al. used a three-dimensional shape optimisation computational tool to obtain a hip stem with improved stability and reduced stress shielding. Various design variables were considered to define the geometric parameterisation of the stem, starting from the Tri-Lock (DePuy) stem geometry. By minimising three single objective functions targeting tangential displacement on the stem–bone interface, normal contact stress, and stress shielding, they obtained seven optimised stems, which were then used to evaluate long-term performance [32].

3.1.2. Bone and Implant Positioning and Initial Fitting

Many authors created the bone–implant assembly using boolean operations and following surgical guidelines to define the relative poses of the two bodies (Table 1). Experienced orthopaedic surgeons typically perform the virtual implantations into a resected femur model by translating and rotating the solid geometries within the visualised CT data using specific software (e.g., DCMTK MFC, Robert McNeel & Associates) [28]. The bone–stem orientation was determined according to ISO 7206 (Table 1) in a few studies [34,37]. Some models have examined the effect of the initial fitting scenarios or initial bone–implant contact area on the bone ingrowth prediction [29,32,41,42]. A perfect initial press fit is what surgeons desire (approximately equal to perfect primary stability) while operating; however, in clinical practice, the stem is often placed with small misalignments while inserted into the bone. To mimic these varying initial contact conditions, M. Tarala et al. generated a gap area of 21% after initially creating a node-to-node surface mesh of bone and implant and adjusting the intramedullary canal contour to match regions with lower local CT values [28]. In another study [41], initial interface contact areas of 100%, 68%, 51%, and 35% with different magnitudes of interfacial gaps ranging from 0 to 1 mm were simulated. Their findings indicated that the ingrowth process accelerated as the contact area between the implant and bone increased. This aligns with another study from M. Viceconti et al. [29], highlighted that a perfect fit configuration led to improved long-term stability through extensive osseointegration. They investigated five initial implant positioning configurations: perfect fit, proximal fit, distal fit, varus fit and valgus fit, which are commonly observed in clinical practice. Two valgus-fitting surgical approaches were also modelled by M. Viceconti et al. in [42]: the implant with proximal lateral and posterior support reached better osseointegration than the configuration that considered the implant with proximal lateral and anterior support. R.B. Ruben et al. [32] clearly stated that totally coated stems are more sensitive to implant misalignments; their results showed that small varus and valgus rotations might lead to reductions in long-term bone ingrowth.

3.1.3. Materials
Bone

Most collected studies assumed the bone as a linearly elastic, heterogeneous, locally isotropic material [27–29,34–36,39–42,47,51,52]. Some assigned constant Young's modulus values for the cortical and trabecular bones [29,32,36,37,40,42,47]. Bonemat [53] or other in-house software is commonly used for the mechanical property mapping step. Hounsfield Unit values are typically extracted from calibrated CT data to estimate local bone mineral density, and non-linear density-to-elasticity relationships are commonly used to compute the elastic modulus, which is then assigned to mesh elements [28,35,41,51].

Anisotropic material properties assumptions were used for cortical bone by H. Mehboob et al. [37], which provide the Young's modulus and Poisson's ratio in radial,

circumferential, and longitudinal directions. F. Tarlochan et al. [33] assigned the anisotropic properties of the cortical bone in longitudinal directions. In addition, few studies [30,31,38,40] considered bone remodelling based on the asymptotic homogenisation method (Table 1). Bone material adaptation, bone remodelling algorithms, or soft tissue differentiation properties will be discussed in the part about the bone–implant interface afterwards.

The effect of bone quality on the long-term fixation of the femoral implants was investigated in [40,41]. Models with superior bone quality indicated larger areas of bone ingrowth, higher rates of ingrowth, and less fibrous tissue. To account for varying bone quality, P. Büchler et al. [40] assigned three different Young's Modulus values for the trabecular bone. In healthy bone, only limited propagation of fibrous tissue was observed in the proximal part of the femur, while poorer bone density showed a thick fibrous membrane around the implant. M. Tarala et al. [41] defined three bone qualities based on the original calcium equivalent distribution. They found that the area of bone ingrowth over the entire interface was higher when better bone quality was considered.

Implant

Most models directly assign commonly used mechanical material properties to the implant, such as Titanium, Cobalt-Chromium, or Stainless steel (Table 1). P. Moreo et al. [38] compared the simulation results obtained considering different hip implant materials and found that stem stiffness has an important effect on bone ingrowth distribution. In particular, they found that flexible stems result in larger areas of poor osseointegration, predominantly observed at the proximal side. J. Folgado et al. [30] found that the CoCr model stem resulted in greater bone resorption compared to titanium stems.

Some modelled the composite construct stem with porous microstructures [28,37]. M. Tarara et al. developed a composite construct stem based on the VerSys Epoch FullCoat design, which includes the neck, inner, middle, and outer layers with various materials for each part [28]. In total, five types of composite materials were tested. Among them, the 80% porosity tantalum with an inner CoCrMo core showed considerably better performance in terms of bone ingrowth and bone remodelling. H. Mehboob et al. [37] studied solid CoCr alloy, Ti alloy stems, and two porous Ti stems and concluded that high-stiffness stems exhibited increased stress shielding and reduced micromotions compared to stems with lower stiffness.

The surface roughness and coating were modelled in some cases considering different mechanical properties like friction coefficient values [26,29–32] and surface material stiffness [38,52]. P. Moreo et al. [38] studied the impact of polished and rough surface finishes on a titanium stem stability, with different sets of interface mechanical properties. They found that rough stems achieved stability sooner than polished stems, while polished stems showed a higher average bonding degree. Few studies have examined the effect of coated and uncoated stems on long-term implant stability. The uncoated stem exhibited less bone resorption at the proximal femur than coated stems of similar geometry with bone ingrowth [30]. Non-uniform bone ingrowth on the coated surfaces was also observed in [26,30–32]. No correlations were found between bone in-growth pattern and coating length for tapered stems [31].

3.1.4. Mesh

Tetrahedral and hexahedral meshes are typically used to build the FE models. Element edge lengths ranging from 0.2 to 3.0 mm and from 0.5 to 4 mm, with a relative finer mesh at the bone–implant interface, were considered in [27] and [35], respectively. In [37], a uniform mesh size of 2 mm was adopted after conducting a mesh sensitivity study. In their study, R. Ghosh et al. [34] also conducted a mesh sensitivity analysis, taking into account the convergence of stress and strain. Peak deviatoric strain was also monitored as part of the convergence check as a robust indicator of tissue growth at the bone–implant interface. They determined the optimal mesh size by considering the implanted femur under peak joint loads during normal gait. X. Liu et al. [48] investigated three different mesh densities with average edge element sizes of 95, 24, and 6 μm, and they found no significant effect of element size on the bone ingrowth fractions.

Table 1. Articles included in the review and summary of the main FE modelling characteristics. Highlighted rows refer to those studies that considered a model that only included the adjacent regions of the bone–implant interface.

Research Paper	Geometry		Virtual Implantation and Stem Pose	Materials		Mesh
	Bone	Implant		Bone	Implant	
P.R. Fernandes et al. [31] 2002	Standard human femur [54]	Tri-Lock Prosthesis of DePuy	NA	Cortical bone: E = 20 GPa; Trabecular bone: orthotropic porous material described with the homogenisation method [55,56]	Titanium (115 GPa)	Hexahedral element
P. Büchler et al. [40] 2003	Three-dimensional hollow cylinder	Truncated cone	Implant placed in the central part of the bone	Cortical bone: E = 15 GPa; Trabecular bone: E = 294, 216, 150 MPa; $v = 0.3$	E = 200 GPa; $v = 0.3$	8-node hexahedral elements
M. Viceconti et al. [29] 2004 (a)	Standard human femur	AncaFit, Cremascoli Ortho, Italy	Implanted by an expert surgeon	Cortical bone: E = 14.2 GPa; Trabecular bone: E = 69 MPa [57]	Titanium Alloy (E = 107 GPa) [57]	Three separate structured hexahedral meshes for the cortical bone, spongiosa, and implant
M. Viceconti et al. [42] 2004 (b)	CT scans of a composite femur [57]	AncaFit, Cremascoli Ortho, Italy	Implanted by an expert surgeon	Cortical bone: E = 14.2 GPa; Trabecular bone: E = 69 MPa [57]	Titanium Alloy (E = 107 GPa) [57]	Structured mesh with 8-node isoparametric hexahedral elements
P. Moreo et al. [38] 2007	Subject-specific CT-scan dataset (middle-aged female)	Commercial design from Zweymüller (AlloPro, Baar, Switzerland)	NA	Anisotropic and heterogeneous	Stainless Steel (E = 210 GPa); Titanium (E = 84 GPa); Polyacetal (E = 20 GPa)	Hexahedral and wedge linear elements
X. Liu et al. [48] 2008	2D model of a plane	Rigid beads and a rigid bottom surface represent the prosthesis substrate	NA	Mature bone: E = 6 GPa; Immature bone: E = 1 GPa	NA	4-node plane strain elements; three mesh densities
A. Lutz et al. [50] 2009	Subject-specific CT-scan dataset	Mayo prosthesis (Zimmer, Germany)	NA	Linear elastic and isotropic, one phase continuum. Constitutive relationship between E and bone mineral density	NA	Linear tetrahedra; wedge elements for the interface layer; mesh refined gradually surrounds the implant model

Table 1. *Cont.*

Research Paper	Geometry		Virtual Implantation and Stem Pose	Materials		Mesh
	Bone	Implant		Bone	Implant	
S. Checa et al. [47] 2009	Cube (3 × 3 × 1 mm)	Cube (3 × 3 × 1 mm)	NA	Cortical bone: Homogeneous, isotropic, and linear elastic (E = 17 GPa; v = 0.3); Immature bone: E = 1 GPa, v = 0.3	Homogeneous, isotropic, and linear elastic (E = 100 GPa; v = 0.3)	Poroelastic elements
J. Folgado et al. [30] 2009	Standard human femur [54]	Tapered-wedge shaped prosthesis (Tri-lock by DePuy; Warsaw, Indiana); Cylindrical cross-sectioned stem (AML by DePuy; Warsaw, Indiana)	Perfect initial fit between the bone and the stem was determined based on post-operative CT scans of two patients following implantation	Trabecular bone: orthotropic, porous, described with the homogenisation method [55,56] Cortical bone: E = 20 GPa	Titanium (E = 115 GPa); Co–Cr alloy (E = 230 GPa), v = 0.3	Hexahedral meshes
P.K. Puthumanapully et al. [35] 2011	Subject-specific CT-scan dataset (43-year-old male)	Commercial design from the Proxima (DePuy)	Surgical instructions	Linearly elastic, heterogeneous, and isotropic;E was assigned using BONEMAT	Titanium alloy Titanium alloy 110 GPa, linear, elastic, isotropic material	First-order tetrahedral elements (edge length: range from 0.5 to 4 mm)
M. Tarala et al. [28] 2011	Subject-specific CT-scan dataset (81-year-old male)	Commercial design from VerSys Epoch FullCoat (Zimmer)	Expert surgeon guidance; in-house software within the visualised CT data (DCMTK MFC 10.8)	Isotropic; properties derived from calibrated CT data using an in-house software package	Five configurations with a layered structure varying material property composition	Linear 4-node tetrahedral elements
R.B. Ruben et al. [32] 2012	Standard human femur [54]	3D shape optimisation model based on the Tri-Lock Prosthesis of DePuy	Sensitivity to misalignments is analyzed	Bone marrow (E = 10^{-7} GPa), trabecular (E = 1 GPa) and cortical bone (E = 17 GPa); v = 0.3	Titanium (E = 115 GPa; v = 0.3)	Hexahedral meshes
A. Andrade-Campos et al. [26] 2012	Human femur	Commercial design from Tri-lock©/Dual-Lock© of DePuy	Follow surgical instructions; rasps are used to shape the hollow femur to fit the shape of the stem	Trabecular bone: Orthotropic, apparent material described with homogenisation [58] at microscopic level; Cortical bone: E = 20 GPa, v = 0.3	Titanium (E = 115 GPa)	Linear hexahedral elements; remeshing technique after virtual implantation

Table 1. *Cont.*

Research Paper	Geometry		Virtual Implantation and Stem Pose	Materials		Mesh
	Bone	Implant		Bone	Implant	
A. Lutz et al. [52] 2012	Subject-specific CT-scan dataset	Commercial design from Metha–prosthesis (Aesculap, Tuttlingen, Germany)	NA	Isotropic; power law for the constitutive relationship between Young's modulus and bone mineral density	Titanium (E = 105 GPa)	Linear tetrahedral elements
M. Tarala et al. [41] 2013	Subject-specific CT-scan dataset (81-year-old male)	VerSys Epoch FullCoat stem (Zimmer, Inc., Warsaw, IN, USA)	The stem was considered settled when a converged subsidence was achieved, meeting the criterion of incremental subsidence values being less than 1% of the total subsidence in subsequent loading periods	Elastic modulus of the bone is computed from the local ash density. Young's Modulus ranged up to 7 GPa, 13.7 GPa, and 22.6 GPa	CoCrMo (E = 240 GPa), PEEK (E = 3.4 GPa) and Fiber mesh (E = 6.9 GPa), $v = 0.3$	4-noded tetrahedral elements
F. Tarlochan et al. [33] 2018	Simplified cylindrical 3D models	Cylindrical shape with homogenous and graded porous microstructure	Interface fit introduced using a prosthesis larger than the bone inner	Cortical bone: anisotropic [59]; Trabecular bone: isotropic (E = 400 MPa)	Isotropic elastic, Ti Alloy (E = 110 GPa), $v = 0.3$	Bones and calluses: 8-node poroelastic element; beads and prosthesis: 8-node solid element
S. Chanda et al. [27] 2020	Subject-specific CT-scan dataset (31-year-old)	Tri-Lock (DePuy) design; One optimal stem model based on a shape optimisation study	Expert surgeon guidance	Linearly elastic, heterogeneous, and isotropic;E assigned using BONEMAT v2	Titanium alloy (E = 110 GPa)	10-node tetrahedra, with the interface having a relatively finer mesh (edge length ranges from 0.2 to 3.0 mm)
R. Ghosh et al. [36] 2020	3D macro-textural models of the only bone-implant interface. Three types of macro-textures based on CLS Spotorno, CORAIL and SP-CL stems		NA	Linear, elastic, homogeneous, and isotropic; (E = 500 MPa, $v = 0.3$)	Linear, elastic, homogeneous and isotropic material (E = 210 GPa, $v = 0.3$)	8-noded hexahedral elements (edge length: maximum 1 mm)
H. Mehboob et al. [37] 2020	Subject-specific CT-scan dataset	3D printed stem	Stems were implanted in the femur and positioned according to the ISO 7206-8: 1995 [60]	Trabecular bone: Isotropic; Cortical bone: anisotropic	CoCr alloy 230 GPa; Ti alloy 110 GPa; 30% porosity Ti 53.8 GPa; 47% porosity Ti 31.5 GPa	Quadratic tetrahedron elements (edge length: 2 mm)

Table 1. *Cont.*

Research Paper	Geometry		Virtual Implantation and Stem Pose	Materials		Mesh
	Bone	Implant		Bone	Implant	
B. Mathai and S. Gupta [51] 2022	Subject-specific CT-scan dataset (31-year-old male); proximal femur	Commercial design from Tri-lock (DePuy); Microscale model to mimic porous surface coating	Expert surgeon guidance; virtually into the resected femur	Linearly elastic, heterogeneous and isotropic; E assigned using BONEMAT v2.0	Titanium alloy (E = 110 GPa, v = 0.3)	10-node tetrahedral elements; (edge length: range from 0.3 to 0.8 mm)
R. Ghosh et al. [39] 2022	3D macro-textural models of the only bone-implant interface.; two different macro-textured implant surfaces based on CORAIL and SP-CL stems		NA	Linear, elastic, homogeneous, and isotropic; (E = 500 MPa, v = 0.3)	A high-nitrogen stainless steel alloy M30NW (E = 195 Gpa), v = 0.3	Linear elastic eight-node hexahedral elements
R. Ghosh et al. [34] 2023	Subject-specific CT-scan dataset (35-year-old female)	Implant model (CORAIL AMT hip stem) with and without macro-textures	Bone–implant assembly created using boolean operation and following surgical protocols. Orientation of the implanted femur based on the ISO 7206-4:2010 [61]	Linearly elastic, heterogeneous, and isotropic; E was assigned using BONEMAT	High-nitrogen stainless steel alloy (E = 195 GPa)	10-noded tetra elements finer mesh at the bone-implant interface region

3.2. Boundary Conditions

A distinction between macroscale, microscale, and hybrid techniques has been made when detailing the boundary conditions for the selected FE modelling studies (Table 2). In particular, macroscale techniques are referred to for those studies where the level of modelling concerns the overall behaviour of the implant–femur structure, while all the works that considered a model that only included the adjacent regions of the bone–implant interface were classified as microscale models (highlighted rows in Table 1).

In macroscale models (Figure 2a), loading conditions are typically determined based on the subject's body weight and applied as hip contact forces and muscular loads (Table 2). Muscle loads are distributed over the respective attachment areas [51] or considered rigid plates attached to the stem and femur to avoid stress concentration [37], while the hip contact forces are usually applied as a concentrated load to the centre of the head of the femoral stem [34,37]. Torsional loading applied to the superior part of the implant was considered in [40]. The femur is usually constrained at the distal part after defining a specific distance *h* below the implant tip (e.g., 45 or 50 mm) (Figure 2) [34,51]. The conditions prescribed by Saint-Venant's principle were checked by [50,52]. Forces and moments extracted from daily activities such as normal walking, stair climbing, standing up, and sitting down are considered in the majority of the selected studies with reference to the work conducted by G. Bergmann et al. [62], M.O Heller et al. [63,64] and D.R Pedersen et al. [65]. Most of the studies considered static loading scenarios [26–32,34,35,37,38,40,42] or solved a quasi-static problem by discretizing the load history into sub-steps of static loading [50,52]. Some authors have proposed adding a less-loaded phase to mimic the resting period or walking with a walking aid after the operation [34,37,38,41]. For example, in [41], an unloading phase was included in each loading cycle with a compressive force of 50 N considered for stability purposes. In the study conducted by [34,37], both muscle and hip forces were reduced in the first simulation period (e.g., 1–8 iterations) considering 80% of the patient's BW and swing phase of the gait cycle. P. Moreo et al. [38] introduced a one-week period of no loading before simulating 25 weeks of healthy activities, where four different loading cases, including resting, were considered. In addition, the frequency of various activities has been taken into account in a few studies [35,38].

The microscale models are usually solved under loading conditions, in terms of both loads and displacements, applied to the implant part while constraining the bone [36,39,47]. In [48], the fixed part was the bottom surface of the implant. Shear load or tangential displacements were typically used to impose relative motion between the bone and the implant, while compressive force or normal displacement were applied to simulate gap distance and press-fit conditions at the bone–implant interface [36,39].

A hybrid approach was adopted in [37,51], where loading conditions applied to the microscale model were obtained by first solving the macroscale analysis (Table 2).

Some authors investigated how different loading conditions could influence the simulation results in terms of osseointegration [34,38,39,52]. R. Ghosh et al. [34] examined the influence of two typical loading scenarios (i.e., normal walking and stair climbing) on the growth of the connective tissue phenotypes (i.e., mesenchymal stem cells, fibrous tissue, cartilage, and bone) around the stem. The results demonstrated a higher occurrence of fibrous tissue during stair climbing in comparison to normal walking. This suggests an increased risk of early AL during stair climbing, potentially attributed to elevated torsional moments at the bone–implant interface. With a higher value of normal displacement at the local interface, an increasing formation of fibrous tissue near the implant surface was found, which might lead to a higher AL risk [44]. R. Ghosh et al. [44] did a full factorial analysis to simulate all the possible combinations of tangential and normal micromotions while assessing their influence on bone growth. They found that both shear and normal micromotion played an important role in the type and amount of tissue phenotype formed at the interface. P. Moreo et al. [38] investigated the influence of patient resting schemes on osseointegration. Three post-surgical scenarios were tested, varying the duration of the initial resting time and load values representing the resting phase included in the

four post-operation activities. The results obtained after simulating 25 weeks post-surgery showed that models with longer initial resting times achieved bone ingrowth stability sooner, while shorter initial resting times showed a lower average bonding degree. A. Lutz et al. [52] studied the effect of discretization of the six load cases on the simulation results. After observing similar patterns in terms of stimulus for osseointegration and corresponding micromotion at the interface obtained considering 180, 90, 45, 30, 15, 10, and 5 load steps, they decided to use only 5 load steps for the simulation in order to reduce the computation cost.
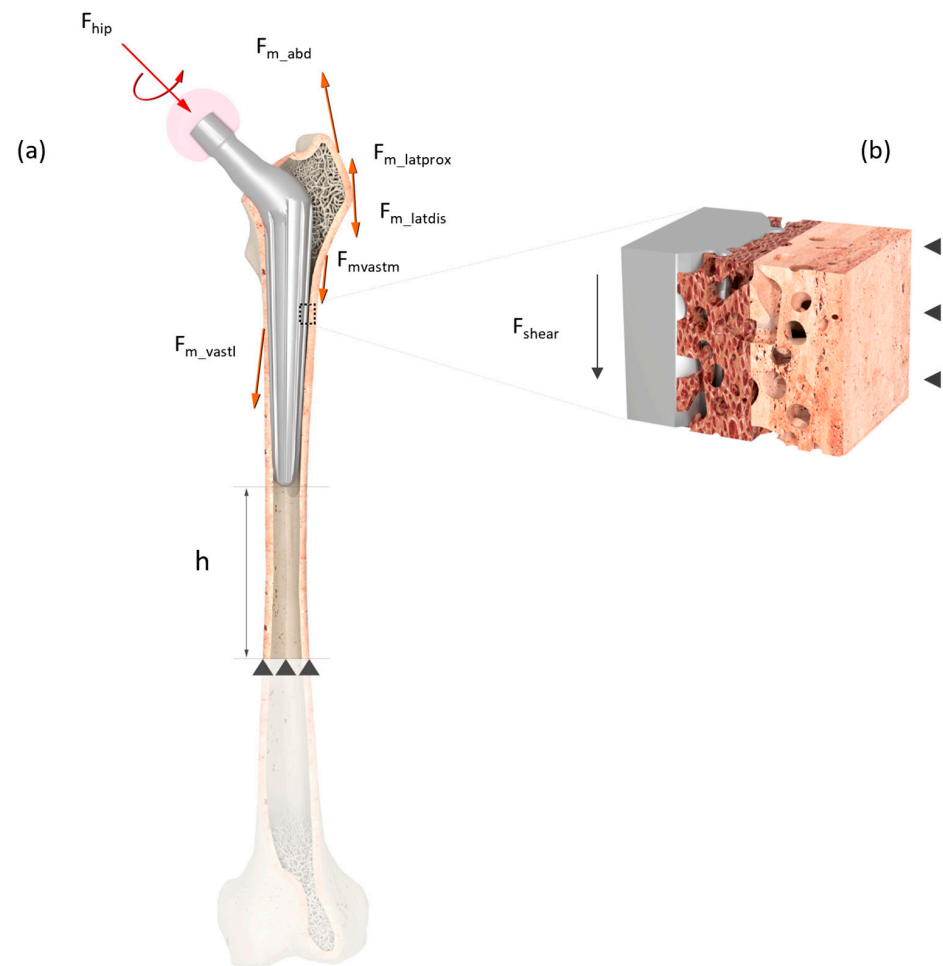
Figure 2. (**a**) Commonly used loading and constrained conditions for the macroscale models. For simplicity, only the main forces involved in normal walking and stair climbing are shown: F_{hip} (hip joint force), F_{m_abd} (abductor), F_{m_vastm} (vastus medialis), F_{m_vastl} (vastus lateralis), $F_{m\_latprox}$ (tensor fascia lata—proximal part), and F_{m_latdis} (tensor fascia lata—distal part). (**b**) Boundary conditions typically defined for microscale models include shear loads or tangential displacements (F_{shear}) at the implant part and constraints at the bone surfaces.

Table 2. Loading conditions defined in the FE modelling studies considering macroscale, microscale, and hybrid techniques.

Macroscale Models		Microscale Models	
Research Paper	Loading Conditions	Research Paper	Loading Conditions
P.R. Fernandes et al. [31] J. Folgado et al. [30] R.B. Ruben et al. [32] A. Andrade-Campos et al. [26]	Peak joint forces during the stand phase of normal walking and the maximal joint load during stair climbing [66]. Muscle force considering one attachment point and hip contact forces.	X. Liu et al. [48]	Combination of 5 MPa shear and 5 MPa compressive stress, corresponding to the maximum load along the length of the stem [67] was applied to the bone part of the model. Beads and the bottom surface of the implant were fixed.
P. Büchler et al. [40]	Torsional loading applied to the superior part of the implant as described in [68].	S. Checa et al. [47]	Both force- and displacement-controlled conditions were used. The bone surface is constrained. Equal pore pressure and nodal displacements on the upper and lower surfaces to approximate a repeating unit of a long implant. Under force controlled conditions, shear load, applied to the implant surface, is defined based on specific initial relative displacements (117–233 μm) between the bone and the implant resulting [69,70].
M. Viceconti et al. [29]	Peak joint load during stair climbing [62] applied as hip contact force.		
M. Viceconti et al. [42]	Model details are reported in [57], where stair-climbing activities are simulated considering a torsional force applied to the implant neck.		
P. Moreo et al. [38]	Four different post-operation activities, including resting, were considered for the load cases. Abductor muscle and hip contact forces [62,64] were applied as two static loads.	R. Ghosh et al. [36]	Tangential displacement of 20 μm applied to the bottom surface of the implant based on [71]. Normal displacement of 20 μm is also applied to simulate press-fit conditions. Top surface of the bone is fixed.
A. Lutz et al. [50] A. Lutz et al. [52]	Different daily activities are considered with load values extracted from the OrthoLoad database. Load history is applied at the hip joint by discretizing the time series into static steps. Nine muscle forces are applied as static equivalent loads [72].	R. Ghosh et al. [39]	Shear displacement (20 μm) and normal displacements (5, 10, 20, 40 μm) applied at the bottom surface of the implant to simulate micromotions at the interface and gap varying, respectively. The top surface of the bone is fixed.
P.K. Puthumanapully et al. [35]	Maximum loads during normal walking and stair climbing. Applied contact hip and muscle forces were extracted from [62]		
M. Tarala et al. [28]	Normal walking loading conditions [64].		
M. Tarala et al. [41]	Four load increments (peak walking force, unloading, peak stair climbing force, and again unloading) are considered in each loading cycle that simulates 4 weeks in situ.		

Table 2. *Cont.*

Macroscale Models		Microscale Models	
Research Paper	**Loading Conditions**	**Research Paper**	**Loading Conditions**
S. Chanda et al. [27]	Maximum loads during the stance phase of normal walking and stair climbing [62,64] are applied as two static load steps. Types of loads: muscles and hip contact forces.		
H. Mehboob et al. [37]	Maximum loads during normal walking [63,65] applied as muscle forces and joint loads at the centre of the head stem. Post-operative conditions are considered.		
R. Ghosh et al. [34]	Maximum loads during normal walking and stair climbing [63,65] applied as muscle forces and joint loads at the centre of the head stem. Post-operative conditions are considered.		
Hybrid Models			
Research paper	**Loading Conditions for the macroscale model**	**Loading Conditions for the microscale model**	
F. Tarlochan et al. [33]	Prosthesis is coaxially fixed using the interference press fit function, and the distal part of the bone is fixed. Loads are applied to the proximal end of the stem, representing the highest reaction forces of physiological body weight and muscular forces during the stance phase of the gait cycle.	External surfaces of the bone fixed. Load applied to the implant part in the longitudinal direction and defined to match the initial micromovements obtained from the micromodel (12–25 μm). Pressure that mimics interference press fit is applied at the bottom surface of the implant.	
B. Mathai and S. Gupta [51]	Maximum loads during the stance phase of four different daily activities are applied as muscle forces and joint forces.	Horizontal and vertical relative displacements were applied at the top bone surface. Values were obtained as average results from the macroscale model considering the four load cases. Bottom surface of the implant is fixed.	

3.3. Bone–Implant Interface Contact

Predicting the long-term stability of implants requires modelling the complex nature of the bone–implant interface and the biochemical processes that govern bone remodelling and ingrowth. Bone remodelling is frequently conducted by modifying the bone density value of the trabecular bone [30–32], typically using the bone adaptive theory [73]. This process is commonly combined with bone ingrowth using time-dependent adaptive modelling techniques. The fundamental principle of this modelling technique is that parameters of interest in response to the loading cases and initial conditions were calculated and then used to adapt the FE model by modifying parameters such as material properties of the tissue or element contact conditions in each load cycle interval. Depending on the main assumptions made to simulate the growth of bone within the surface of an implant, the selected studies for this review can be classified into two broad categories: Direct Contact models and Indirect Contact models. A summary of interface contact methodologies presented by the different studies belonging to these two categories is reported in Table 3, while the main assumptions are summarised below. The effect of considering different assumptions when estimating bone ingrowth will be discussed in the Discussion section.

3.3.1. Direct Contact

For direct contact models, bone ingrowth is simulated by changing parameter values directly associated with the status of the contact elements at the bone–implant interface. Typical contact statuses are: (i) *bonded*, which simulates perfect osseointegration; (ii) *gap*, representing the presence of fibrous tissue at the interface, and (iii) *frictional*, or *standard*, that reproduces initial post-operative conditions [29,42]. Contact parameters such as contact stiffness [29] and coefficient of friction [42] are used to define the rules considered for the status change. For example, in [29], a fibrous status is obtained with a contact stiffness set to 15 N mm^{-1} [42]. Interface stiffness was also considered in [32] to determine five osseointegration levels. Relative tangential displacement between bone and implant is typically extracted as mechanical stimulus used to drive the change of the contact parameter values (e.g., 50 μm is the micromotion threshold value below which the bounded status is obtained in [30,31]). Tensile stress and contact compressive stress are also considered for bone ingrowth and possible de-bounding [29,32]. Typical coefficient of friction considered between the bone and coated stem for the different contact statuses are: bonded (μ > 0.32), fibrous (μ < 0.0003), and standard (0.0003 ≤ μ < 0.32) [42]. Initial interface conditions are usually set to frictionless for uncoated stems and to frictional contact for coated surfaces (a coefficient of friction of 0.6 or 1.7 in the press-fit condition).

3.3.2. Indirect Contact

For indirect contact models, an extra layer of elements considered between the bone and the stem is used to characterise the bonding strength, for example, by changing the stiffness value of spring elements linking in between [27,28,41] or the mechanical properties of the interface solid elements [35]. In [41], spring elements were activated to simulate bone ingrowth, considering stiffness values obtained from computed local micromotion, gap, and stress values. Spring length is typically defined based on the gap distance between two adjacent interfacial nodes, while stiffness values ranged between 10^{-6} N/mm (the lowest osseointegration level at the initial postoperative condition) and 30 N/mm (the highest level of osseointegration, which corresponds to bounded contact) [27]. An interface layer of solid elements was considered in most of the selected studies (Table 3). Mechanical properties are adjusted for each element to characterise tissue differentiation (e.g., from granulation tissue to fibrous tissue, intermediate bone, immature bone, cartilage, and mature bone), often in accordance with mechano-regulatory models and diffusion analyses of mesenchymal stem cells (MSCs), which differentiate into fibroblasts, chondrocytes, and osteoblasts. These models incorporated specific stimuli as inputs (such as relative tangential displacement at the interface, strain energy density, shear strain, and fluid/solid velocity). Oxygen concentration was considered a mechanical stimulus for tissue differentiation

in [47], and capillary network formation was also included in the simulation. Typical Young modulus values set for the different tissues are: 0.2–1 MPa for granulation; 0.2–5 MPa for fibrous tissue; 5–1000 MPa for cartilage; 1000–6000 MPa for immature bone; and ≥ 2000 for mature bone [74]. Most of the studies used a smoothing process to average the Young modulus values considered for the material properties mapping during the simulations, thus mitigating numerical instabilities [33,48,51]. Typical thickness values considered for the interface layer are 0.2–1 mm. A maximum thickness layer of 5 mm was modelled in the case of macro-textural implant surfaces [36,44]. For most of the indirect contact models that include the interface tissue layer in the proximal part of the implant, bounded contact was assumed between implant tissue surfaces and bone tissue surfaces. Frictional implant bone contact in the distal part of the coated implant was also considered in a few studies (e.g., friction coefficient values in the range 0.5–0.85) [37,51].

3.4. Quantities of Interest

The long term stability of the implant was evaluated in most of the studies by extracting results in terms of bone remodelling and bone ingrowth. In particular, bone density distribution values, or density percentage variation, were recorded during the simulation to assess the bone resorption process of the cancellous bone.

For the direct contact models, temporal evolution and spatial distribution of bounded contact elements are typically extracted to assess the bone osseointegration process [29,31,42]. The percentage of contact elements and the fraction of stem surface belonging to the different contact statuses were recorded for each of the seven Gruen zones in [29].

The percentage of ingrowth area and the spatial distribution of the bonding degree during the simulation were also considered for direct contact models.

As also mentioned in the previous section, typical mechanical stimuli considered to set the contact status or the tissue differentiation conditions are relative micromotions, strain energy density, tensile, and shear stresses at the interface. The quantities of interest were typically extracted at the initial contact configuration, indicating post-operative conditions, and at long-term conditions. The maximum time frame observed for extracting the simulation results was 120 days weeks [36,44].

Table 3. Summary of interface contact methodologies presented by the different studies to model osseointegration at the bone-implant interface. Depending on the main assumptions made to simulate the growth of bone within the surface of an implant, two broad categories are identified: Direct Contact models and Indirect Contact models.

Research Paper	Direct Contact Models
P.R. Fernandes et al. [31]	Bone remodelling was simulated by changing the bone density of the trabecular bone and contact conditions after solving an optimisation problem that considered structural compliance and total bone volume. Initial interface conditions were set to contact with a friction coefficient of 1.7 for coated surfaces and frictionless contact for uncoated surfaces. After the first iterations, relative displacement was computed for each contact node, and if the value was <50 µm, bone ingrowth was simulated by changing the contact status at that node to bonded. Once a node is set to bond, it will remain until the end.
P. Büchler et al. [40]	Fibrous tissue formation is based on a differential equation that includes three parameters: the rate of biological evolution v and two threshold values indicating shear strains that promote the formation, ε_{min}, of bone tissue or fibrous tissue, ε_{max}. The parameters were determined to match the same thickness of fibrous tissue value obtained with experimentally observed micromotion of 20 and 150 µm after 3 weeks of evolution [68]: $\varepsilon_{min} = 2.3 \times 10^{-3}$, $\varepsilon_{max} = 8.2 \times 10^{-3}$ and $v = 5$ weeks $^{-1}$. The prosthesis was assumed to be in contact with the cancellous bone, with the friction coefficient set to 0.6.
M. Viceconti et al. [29]	The bone–implant interface was modelled with face-to-face frictional contact elements. Osseointegration was simulated using a discrete-states machine. Contact element status is set based on micromotion values d_c: *bonded* if $d_c < 40$ µm; *gap* if $d_c > 150$ µm; *frictional* if 40 µm $< d_c > 150$ µm. *Bonded* condition was implemented by drastically increasing the tangential contact stiffness and the normal contact stiffness. *Gap* status assumed fibrous tissue between bone and implant, which was modelled using the stiffness relaxation technique [75]. A contact stiffness of 15 N mm $^{-1}$ was set to produce a 500 µm gap. *Frictional* status is modelled as an elastic frictional contact. The contact stiffness was set at 3×10^4 N mm $^{-1}$ to ensure peak penetration less than 1 µm. De-bonding was checked after the initial contact settings based on the stress threshold. Elements return to the friction status if: tensile stress > 0.8 MPa or shear stress > 4.9 MPa.
M. Viceconti et al. [42]	The bone–implant interface was modelled with face-to-face frictional contact elements. Osseointegration is simulated using a continuous and rule-based model and described for each time step and generic point at the interface with a first-order model in which the coefficient of friction µ is expressed as a function of the shear stress and micromotion. State of each contact element depends on the friction coefficients: *bonded* (µ > 0.32), *fibrous* (µ < 0.0003), and *standard* (0.0003 ≤ µ < 0.32).
J. Folgado et al. [30]	Bone remodelling was simulated as in [31]. Initial interface conditions were set to contact with a friction coefficient (0.6) for coated surfaces and frictionless contact for uncoated surfaces. After the first iteration, the relative displacement d was computed for each contact node. Two micromotion threshold values ($d < 25$ or < 50 µm) for the bonded contact state were analysed separately.
R.B. Ruben et al. [32]	Bone remodelling was simulated as in [31]. Contact elements changed status with a rule-based algorithm. Bone ingrowth occurs if all these five conditions are satisfied: relative tangential displacement < 25 µm; gap < 150 µm; tensile stress < 0.8 MPa, contact compressive stress < 7.89 MPa; shear stress below threshold values depending on the interface stiffness and related osseointegration level (e.g., shear stress should be less than 4.5 MPa when interface stiffness is zero, which corresponds to osseointegration level 1 and the initial simulated period immediately after surgery). Interface stiffness increases by one level until level 5 is reached, if all criteria are satisfied. Interface stiffness can return to zero if one of the conditions is not satisfied.

Table 3. *Cont.*

Research paper	Indirect contact models
P. Moreo et al. [38]	Bone remodelling and bone ingrowth were simulated based on the theory of continuum damage mechanics. Interface damage or interface repair was modelled by changing tissue stiffness (i.e., bounding degrees) defined based on mechanical stimuli (e.g., relative displacement at the interface). The bonded/debonded process was implemented using thin elements that connect the bone and implant with frictionless contact between the surfaces.
X. Liu et al. [48]	Two models were used to simulate osseointegration. In the first model, the mechano-regulatory model and diffusion analysis described in [76] were used for the differentiation of MSCs into fibroblasts, chondrocytes, and osteoblasts. The new tissue type was predicted for each element, and the effective material properties were assigned based on [76]. The second model used a modified tissue differentiation algorithm that allowed a change from immature bone to mature bone and the reverse change (bone resorption).
A. Lutz et al. [50]	Bone ingrowth was simulated using a linear elastic bioactive interface layer. An evolution rule for osseointegration based on normal pressure and relative motion was considered to change the tissue stiffness.
S. Checa et al. [47]	A lattice model that represents a space for the extracellular matrix and cells was considered for the tissue differentiation algorithm. Cells can proliferate, migrate, and differentiate according to the mechanoregulation algorithm proposed in [43], which also included the growth of the capillaries. Oxygen concentration and two mechanical stimuli, shear strain and fluid/solid velocity, were used for the differentiation of MSCs into fibroblasts, chondrocytes, and osteoblasts. Osseointegration was implemented considering a bone–implant interface layer of 1 mm thick regenerative tissue of poroelastic elements.
P.K. Puthumanapully et al. [35]	A uniform layer of 0.75 mm (corresponding to three layers of porous coating thickness in the Proxima implant) was created around the implant to represent the formation of granulation tissue. This layer was assumed to be fully bonded to the implant and the bone. Tissue differentiation algorithm based on the mechano-regulation theory from Carter et al. [77]. The tendency for ossification was represented by the osteogenic index 'I', dependent on the element stress state at each cycle. A low value of I denotes the tendency to form fibrous tissue. The index was mapped onto a range of material properties, considering an interpolated value of the Young's modulus of the materials. Values were averaged over 10 iterations to avoid rapid changes in tissue type from one iteration to the next. Convergence was obtained after about 50 iteration or when the change in tissue type between two successive iterations in every element in the layer was less than 5%.
M. Tarala et al. [28]	Bone ingrowth simulated by activating spring elements based on micromotion (less than 40 μm); gap value (smaller than 500 μm); local stresses (less than 25 MPa). De-bonding (spring elements deactivated) occurred when local bone stresses exceeded 25 MPa. Frictional implant–bone contact (coefficient was 0.5 or 0.88 for different materials of the stem). The spring stiffness was defined as the summation of the adjacent bone elements' Young's Modulus was multiplied by 1/3 of the corresponding element face area (each face had three nodes connected to it), divided by the original spring length (equal to the gap between implant and bone node). Bone remodelling was simulated only for the cases with the best bone ingrowth performance. Adaptive bone theory was used [73].
A. Andrade-Campos et al. [26]	The bone–implant interface was modelled with a surface-based contact model with the penalty method (the stem is the master surface and the bone is the slave). Bone remodelling was simulated using an optimisation process that computes the evolution of volume fraction (0 void; 1 total density corresponding to cortical bone) at each point based on strain energy density values. Osseointegration was simulated by changing the stiffness of connector elements included between the bone and the stem based on a relative displacement criteria described in [31]. Osseointegration increases when the contact is achieved (normal contact force >1) and the tangential displacement is less than a threshold value. If these conditions were not verified, the initial contact conditions (contact with friction 0.3 if the surface is coated and frictionless contact for uncoated surfaces). Fully osseointegration was modelled with glued contact. De-bounded was also possible for high levels of stress (contact pressure > 0.8 MPa and shear stress > 35 MPa).
A. Lutz et al. [52]	An interface layer made of solid elements is considered between the bone and implant surfaces, with the initial constitutive behaviour described by the Drucker–Prager plasticity model [78]. Osseointegration is simulated considering the evolution of bone mineral density as a function of the mechanical stimuli (micromotions and strain energy density): interface stiffness, ability to carry tensile loads, and the limit until sliding occurs, which increases with ongoing mineralization.

Table 3. *Cont.*

Research paper	Indirect contact models
M. Tarala et al. [41]	Bone ingrowth was simulated by activating spring elements with stiffness based on the ingrowth potential parameter *P*, which was computed based on the local micromotion stress and gap value micromotion (micromotion less than 40μm, gap value smaller than 1 mm, and local stresses less than 25 MPa). A non-linear progression of the spring stiffness was considered with *P*. A complete ingrowth was assumed after four loading periods (*P* = 1) under ideal conditions of micromotion and a gap equal to zero. Frictional implant-bone contact (coefficient 0.5).
F. Tarlochan et al. [33]	Microscale model of porous structures made of titanium alloy was constructed with a fixed RVE (representative volume element). The beads were initially placed inside a granulation tissue (callus) and penetrating the bone. The callus was tied to the bone and the prosthesis surface; sliding contact with a coefficient of friction of 0.4 was used between the beads and the callus and between the bone and the beads. An algorithm based on the biphasic mechano-regulation theory from Isaksson et al. 2006 [74] was used to predict tissue differentiation, including granulation tissue, fibrous tissue, intermediate bone, immature bone, cartilage, and mature bone. According to a stimulus computed using deviatoric strain and fluid flow, the material properties of the callus were updated in each element. A smoothing process was used to average the Young modulus values considered for the material properties mapping during the simulations.
S. Chanda et al. [27]	The bone–implant interface was modelled with large sliding surface-to-surface frictional contact elements. Bone remodelling is simulated using adaptive bone theory [13]. Bone ingrowth is simulated using contact, and spring elements (CONBIN14) are activated when the five conditions described in [32] are satisfied. Initial contact stiffness is assigned to ensure a low penetration [29] and a friction coefficient set to 0.4. Stiffness values for spring elements range between 10^{-6} (osseointegration level 1 at the initial post-operative condition) and 30 N/mm (the highest level of osseointegration, which corresponds to bounded contact). Spring length is defined based on the gap between two adjacent interfacial nodes.
R. Ghosh et al. [36]	A maximum thickness for the granulation tissue of 5 mm was assumed between the implant and the bone. The implant–tissue interface and bone–tissue interface were considered perfectly bonded. The mechano-regulatory model and diffusion analysis described in [76] were used for the differentiation of the MSCs into fibroblasts, chondrocytes, and osteoblasts. The new tissue type was predicted for each element, and the effective material properties were assigned based on [76]. The simulation was carried out for 120 iterations, which corresponded to 120 days.
H. Mehboob et al. [37]	Two tissue layers of 0.5 and 1 mm thick were considered to simulate the granulation tissue (callus) only at the proximal end of the stems. The callus was tied to the bone and stem surface. Ain the distal part, a surface-to surface frictional contact (0.5) was used between the stem and the bone. An algorithm based on the mechano-regulation theory from H. Isaksson et al. [74] was used to predict tissue differentiation. According to a stimulus computed using deviatoric strain, the material properties of the callus were updated for each element. A total of 16 iterations were considered for the entire simulation.
B. Mathai and S. Gupta [51]	An inter-bead granulation tissue of 850 μm was initially modelled with a fixed RVE only at the proximal part of the stem. The beads were assumed to penetrate the bone layer by 5 μm. Fully bonded contact was assumed between the tissue and the surfaces of the implant and bone. At the distal part, the implant-bone interface was modelled using a surface-to-surface contact with a frictional coefficient of 0.85. The tissue differentiation modelling technique presented in [36] was used. A temporal smoothing method was used to average the material properties assigned, avoiding numerical instabilities. The simulation was carried out for 60 iterations, which corresponded to 60 days.
R. Ghosh et al. [39]	A granulation tissue (minimum thickness of 2 mm) was assumed between the implant and the bone. The implant–tissue interface and bone-tissue interface were considered perfectly bonded. The tissue differentiation modelling technique and simulation scheme presented in [36] were used. The simulation was carried out for 120 iterations, which corresponded to 120 days.
R. Ghosh et al. [34]	A layer of granulation tissue (1 mm thick) was included around the proximal stem surface by Boolean subtraction operation. The implant-tissue interface and bone–tissue interface were considered perfectly bonded. In the distal part of the implant, a surface-to-surface contact was modelled between the implant and the bone with a coefficient of friction of 0.5. The tissue differentiation modelling technique presented in [36] was used. The simulation was carried out for 56 iterations, which corresponded to 56 days.

4. Discussion

From this state-of-the-art review of the FE models predicting the AL failure, the main advantages and limitations of the different modelling approaches adopted by various authors have emerged.

One of the most critical aspects when simulating the long-term stability of hip prostheses is modelling the complex osseointegration processes occurring at the femur–implant interface. The adaptative FE model was found to be a widely used technique to simulate osseointegration. Finite Element software such as Ansys and Abaqus was typically coupled with user subroutines programmed in Python or Matlab to iterate and integrate the calculations. Both bone remodelling and bone ingrowth, essential for maintaining the secondary stability of the cementless stem, should be included in the simulations. Since they are related processes in vivo (e.g., bone ingrowth is influenced by factors related to bone remodelling), most FE studies considered a combination of the two implemented within the same workflow loop [26,27,30–32,38,48]. Bone ingrowth and bone remodelling were considered two independent phenomena in a few models [26,28]. "Bone ingrowth" refers to the growth of bone within the irregular surface of an implant or its intimate contact at the bone–implant interface following the biological response. "Bone remodelling" involves the removal of mineralised bone by osteoclasts (bone resorption/bone loss/osteolysis) followed by the formation of bone matrix through the osteoblasts that subsequently become mineralised (bone apposition or bone formation) [79,80]. In this last process, the biological process of cell differentiation, also known as "bone adaptation", plays a crucial role.

It is worth noting that bone remodelling was often simulated as bone mineral loss associated with the so-called stress shielding phenomenon. While bone resorption is indeed a biological process correlated with an increased risk of implant loosening, AL cannot be solely attributed to bone density loss. Therefore, this review focused more on papers that predicted bone ingrowth failure or the combined effects of the two processes.

As also reported in Section 3.3, two main bone interface contact modelling techniques were identified and named as direct contact and indirect contact models. The first are more computationally efficient; however, regarding their main assumptions, some limitations should be pointed out. For example, in a few direct contact models, only one mechanical stimulus controls the change in contact status, and the outcome is such that once the contact behaviour is set to be bonded, it will remain in that state until the simulation process is complete [30,31]. Certain direct contact models addressed this limitation by incorporating additional criteria for debonding checks [29,32]. The indirect contact models involving spring elements also overcome this problem by varying the osseointegration level with different spring stiffness values [27]. The mechano-regulatory models and diffusion analyses of mesenchymal stem cells included in many indirect contact models that considered an interface layer enabled a more realistic mimicry of biological progressions and simulation of tissue differentiation processes [34,36,39,48]. However, most of these models assumed that, even under initial post-operative conditions, the implant is surrounded by a layer of granulation tissue, whereas, in reality, the implant is in direct contact with the bone. Some uncertainties related to the definition of the micromotion threshold value used to estimate bone ingrowth were observed. For example, P.R. Fernandes et al. [31] considered a threshold value of 50 μm below which the contact status was set to bounded. M. Viceconti et al. [29] adopted a similar approach with a 40 μm micromotion threshold value. J. Folgado et al. [30] compared two threshold values of 25 and 50 μm while determining whether the element was bonded or frictional. They showed a significant impact on the prediction of bone ingrowth. Bone ingrowth on the partially coated cylindrical stem was absent when the micromotion criterion was set at 25 μm, but some ingrowth was observed when the criterion was relaxed to 50 μm. Micromotion thresholds of 50, 75, and 100 μm have also been investigated by A. Lutz et al. [52], and it was shown that for higher micromotion thresholds, the predicted osseointegration was also higher.

Some microscale models mimicking only local bone implant interfaces were proposed to investigate osseointegration and reduce the computational cost of the simula-

tion [36,39,47,48]. Although these models can more accurately and efficiently simulate the biochemical processes occurring at the interface, the influence of the anatomical topology of the bone, patient and implant variabilities, or loading scenarios on bone ingrowth would be limited.

Loading cases are another crucial consideration for predicting the long-term stability of the implants. In particular, the iterative computational process necessitates careful selection of load cycle intervals; otherwise, it may yield inaccurate results [81]. Also, as we mentioned above, the loading cases for the microscale models were limited, mainly based on constant shear loads or tangential displacements. The hybrid method proposed in [33,51] represents a good combination of the advantages of both macroscale and microscale modelling approaches: it integrates the results obtained by solving the macroscale model, thereby capturing the overall behaviour of the system, with the loading configuration considered from microscale models. For the macroscale models, the peak value of the hip joint force of normal walking and stair climbing was most widely used. Reducing the number of discretization sub-steps for the hip joint load resulted in accurate mechanical stimulus for osseointegration at the bone–implant interface [52], which could serve as a practical reference when considering methods to reduce computational expense. Although the effect of various loading cases, including different postoperative conditions, on bone ingrowth results has been analysed in a few studies [34,38], we still have limited knowledge regarding which set of loading cases best predicts in vivo conditions. Also, one notable observation is that, to the best of the author's knowledge, no simulation has yet considered an abnormal gait cycle associated with various pathologies or conditions affecting the musculoskeletal system. In the future, it would be meaningful to investigate how abnormal gait patterns affect the results of osseointegration computational models.

One last critical point worth mentioning is model validation. Traditional validation activities typically involve a rigorous comparison of the model predictions with the results obtained from the comparator (i.e., bench testing, clinical trials, animal experiments) [82]. For current bone osseointegration models, the existing literature acknowledges a lack of sufficient experimental and clinical data to robustly validate the computational models [36,51]. Another big challenge for these FE models is not only accurately predicting the osseointegration process in vivo but also determining when it occurs and identifying whether it ultimately caused the implant to loosen. Very few studies provided quantitative comparative evidence in terms of bone ingrowth (e.g., percentage of the osseointegration area, fibrous tissue thickness) between the computational results and the clinical data [29,30,40]. A comparison between the relative micro-movements predicted by the models and the experimental measurements taken in vitro was mentioned in [42]. Qualitative agreement between simulation outputs and clinical observations was often used as model plausibility evidence. For example, a few authors found that bone ingrowth does not occur uniformly across the coated surface but rather partially [26,30,31]. More bone formation was observed on the medio-lateral sides and towards the proximal regions of Gruen zones 2 and 6 [34,35], which is in agreement with the radiographic results from the five-year follow-up study [83]. An interesting Ansys-to-DEXA conversion technique to present simulation results with clinical relevance was described in [27]. This involved converting the density values of the FE elements into two-dimensional pixel grey values and considering the differences in grey values between post-operative and long-term predictions across the seven Gruen zones.

5. Conclusions

In conclusion, the present study provides a comprehensive analysis of the main FE models predicting the AL failure risk induced by the lack of long-term stability. The main modelling assumptions, including bone and implant geometry, materials, boundary conditions, and the bone–implant interface, were summarised and presented. The limitations of various modelling assumptions and their impact on the simulation results were also discussed. Technical differences and trends in methodology evolution have been observed. Specifically, the modelling of long-term stability in femoral stems has progressed from

macroscopic direct contact models to more advanced indirect models integrating interface layers. Microscale or hybrid models, focusing on localised regions at the interface, have grown in complexity, incorporating detailed surface porous structures and sophisticated tissue differentiation algorithms. This progress has been made possible thanks to the growth of available computational resources.

Although several important improvements in computational modelling have been made, it is evident that further advancements are needed. In particular, more rigorous step-by-step clinical validation for osseointegration models would be crucial for translating computational methodologies into clinical practice. Failure criteria used to determine loosening of the implant should be clearly defined, and effort should be made to identify the appropriate limit of tolerable conditions (e.g., maximum micromotion at the interface) considering implant, patient, and environmental factors, as also suggested by [84].

Extra attention should also be paid to the terminology used to present FE studies on AL. Terms such as "bone ingrowth", "bone remodelling" and "bone adaptation" are often used interchangeably to define the osseointegration process since they all include the bone formation description.

References

1. Kurtz, S.M.; Ong, K.L.; Lau, E.; Widmer, M.; Maravic, M.; Gómez-Barrena, E.; de Fátima de Pina, M.; Manno, V.; Torre, M.; Walter, W.L.; et al. International Survey of Primary and Revision Total Knee Replacement. *Int. Orthop.* **2011**, *35*, 1783–1789. [CrossRef] [PubMed]
2. Lübbeke, A.; Silman, A.J.; Barea, C.; Prieto-Alhambra, D.; Carr, A.J. Mapping Existing Hip and Knee Replacement Registries in Europe. *Health Policy Amst. Neth.* **2018**, *122*, 548–557. [CrossRef]
3. Singh, J.A.; Yu, S.; Chen, L.; Cleveland, J.D. Rates of Total Joint Replacement in the United States: Future Projections to 2020–2040 Using the National Inpatient Sample. *J. Rheumatol.* **2019**, *46*, 1134–1140. [CrossRef]
4. Rupp, M.; Lau, E.; Kurtz, S.M.; Alt, V. Projections of Primary TKA and THA in Germany from 2016 through 2040. *Clin. Orthop.* **2020**, *478*, 1622–1633. [CrossRef] [PubMed]
5. Yamada, H.; Yoshihara, Y.; Henmi, O.; Morita, M.; Shiromoto, Y.; Kawano, T.; Kanaji, A.; Ando, K.; Nakagawa, M.; Kosaki, N.; et al. Cementless Total Hip Replacement: Past, Present, and Future. *J. Orthop. Sci.* **2009**, *14*, 228–241. [CrossRef]
6. Toossi, N.; Adeli, B.; Timperley, A.J.; Haddad, F.S.; Maltenfort, M.; Parvizi, J. Acetabular Components in Total Hip Arthroplasty: Is There Evidence That Cementless Fixation Is Better? *J. Bone Joint Surg. Am.* **2013**, *95*, 168–174. [CrossRef]

7. Report of RIPO Overall Data on Hip, Knee and Shoulder Arthroplasty in Emilia Romagna Region (Italy, 2000–2019). 2022. Available online: https://ripo.cineca.it/authzssl/pdf/Annual%20report%202019%20RIPO%20Register_v2.pdf (accessed on 13 May 2022).
8. *National Joint Registry 20th Annual Report 2023*; Healthcare Quality Improvement Partnership Ltd.: London, UK, 2023.
9. Iamthanaporn, K.; Chareancholvanich, K.; Pornrattanamaneewong, C. Revision Primary Total Hip Replacement: Causes and Risk Factors. *J. Med. Assoc. Thail. Chotmaihet Thangphaet* **2015**, *98*, 93–99.
10. Sadoghi, P.; Liebensteiner, M.; Agreiter, M.; Leithner, A.; Böhler, N.; Labek, G. Revision Surgery after Total Joint Arthroplasty: A Complication-Based Analysis Using Worldwide Arthroplasty Registers. *J. Arthroplast.* **2013**, *28*, 1329–1332. [CrossRef]
11. Ferguson, R.J.; Palmer, A.J.; Taylor, A.; Porter, M.L.; Malchau, H.; Glyn-Jones, S. Hip Replacement. *Lancet* **2018**, *392*, 1662–1671. [CrossRef]
12. Anil, U.; Singh, V.; Schwarzkopf, R. Diagnosis and Detection of Subtle Aseptic Loosening in Total Hip Arthroplasty. *J. Arthroplast.* **2022**, *37*, 1494–1500. [CrossRef]
13. Janssen, L.; Wijnands, K.A.P.; Janssen, D.; Janssen, M.W.H.E.; Morrenhof, J.W. Do Stem Design and Surgical Approach Influence Early Aseptic Loosening in Cementless THA? *Clin. Orthop.* **2018**, *476*, 1212–1220. [CrossRef] [PubMed]
14. Keurentjes, J.C.; Pijls, B.G.; Van Tol, F.R.; Mentink, J.F.; Mes, S.D.; Schoones, J.W.; Fiocco, M.; Sedrakyan, A.; Nelissen, R.G. Which Implant Should We Use for Primary Total Hip Replacement? A Systematic Review and Meta-Analysis. *J. Bone Joint Surg. Am.* **2014**, *96* (Suppl. S1), 79–97. [CrossRef] [PubMed]
15. Havelin, L.I.; Espehaug, B.; Vollset, S.E.; Engesaeter, L.B. Early aseptic loosening of uncemented femoral components in primary total hip replacement. A review based on the Norwegian Arthroplasty Register. *J. Bone Joint Surg. Br.* **1995**, *77*, 11–17. [CrossRef] [PubMed]
16. Wagner, M.; Schönthaler, H.; Endstrasser, F.; Dammerer, D.; Nardelli, P.; Brunner, A. Mid-Term Results After 517 Primary Total Hip Arthroplasties With a Shortened and Shoulderless Double-Taper Press-Fit Stem: High Rates of Aseptic Loosening. *J. Arthroplast.* **2022**, *37*, 97–102. [CrossRef] [PubMed]
17. Hoskins, W.T.; Bingham, R.J.; Lorimer, M.; de Steiger, R.N. The Effect of Size for a Hydroxyapatite-Coated Cementless Implant on Component Revision in Total Hip Arthroplasty: An Analysis of 41,265 Stems. *J. Arthroplast.* **2020**, *35*, 1074–1078. [CrossRef]
18. Graudejus, O.; Ponce Wong, R.; Varghese, N.; Wagner, S.; Morrison, B. Bridging the Gap between in Vivo and in Vitro Research: Reproducing in Vitro the Mechanical and Electrical Environment of Cells in Vivo. *Front. Cell. Neurosci.* **2018**, *12*. [CrossRef]
19. AKHTAR, A. The Flaws and Human Harms of Animal Experimentation. *Camb. Q. Healthc. Ethics* **2015**, *24*, 407–419. [CrossRef] [PubMed]
20. Viceconti, M.; Affatato, S.; Baleani, M.; Bordini, B.; Cristofolini, L.; Taddei, F. Pre-Clinical Validation of Joint Prostheses: A Systematic Approach. *J. Mech. Behav. Biomed. Mater.* **2009**, *2*, 120–127. [CrossRef]
21. Taylor, M.; Prendergast, P.J. Four Decades of Finite Element Analysis of Orthopaedic Devices: Where Are We Now and What Are the Opportunities? *J. Biomech.* **2015**, *48*, 767–778. [CrossRef]
22. Taylor, M.; Bryan, R.; Galloway, F. Accounting for Patient Variability in Finite Element Analysis of the Intact and Implanted Hip and Knee: A Review. *Int. J. Numer. Methods Biomed. Eng.* **2013**, *29*, 273–292. [CrossRef]
23. Viceconti, M.; Emili, L.; Afshari, P.; Courcelles, E.; Curreli, C.; Famaey, N.; Geris, L.; Horner, M.; Jori, M.C.; Kulesza, A.; et al. Possible Contexts of Use for In Silico Trials Methodologies: A Consensus-Based Review. *IEEE J. Biomed. Health Inform.* **2021**, *25*, 3977–3982. [CrossRef]
24. Favre, P.; Maquer, G.; Henderson, A.; Hertig, D.; Ciric, D.; Bischoff, J.E. In Silico Clinical Trials in the Orthopedic Device Industry: From Fantasy to Reality? *Ann. Biomed. Eng.* **2021**, *49*, 3213–3226. [CrossRef] [PubMed]
25. Pankaj, P. Patient-Specific Modelling of Bone and Bone-Implant Systems: The Challenges. *Int. J. Numer. Methods Biomed. Eng.* **2013**, *29*, 233–249. [CrossRef] [PubMed]
26. Andrade-Campos, A.; Ramos, A.; Simões, J.A. A Model of Bone Adaptation as a Topology Optimization Process with Contact. *J. Biomed. Sci. Eng.* **2012**, *5*, 229–244. [CrossRef]
27. Chanda, S.; Mukherjee, K.; Gupta, S.; Pratihar, D.K. A Comparative Assessment of Two Designs of Hip Stem Using Rule-Based Simulation of Combined Osseointegration and Remodelling. *Proc. Inst. Mech. Eng. Part H* **2020**, *234*, 118–128. [CrossRef]
28. Tarala, M.; Janssen, D.; Verdonschot, N. Balancing Incompatible Endoprosthetic Design Goals: A Combined Ingrowth and Bone Remodeling Simulation. *Med. Eng. Phys.* **2011**, *33*, 374–380. [CrossRef] [PubMed]
29. Viceconti, M.; Pancanti, A.; Dotti, M.; Traina, F.; Cristofolini, L. Effect of the Initial Implant Fitting on the Predicted Secondary Stability of a Cementless Stem. *Med. Biol. Eng. Comput.* **2004**, *42*, 222–229. [CrossRef] [PubMed]
30. Folgado, J.; Fernandes, P.R.; Jacobs, C.R.; Pellegrini, V.D. Influence of Femoral Stem Geometry, Material and Extent of Porous Coating on Bone Ingrowth and Atrophy in Cementless Total Hip Arthroplasty: An Iterative Finite Element Model. *Comput. Methods Biomech. Biomed. Eng.* **2009**, *12*, 135–145. [CrossRef]
31. Fernandes, P.R.; Folgado, J.; Jacobs, C.; Pellegrini, V. A Contact Model with Ingrowth Control for Bone Remodelling around Cementless Stems. *J. Biomech.* **2002**, *35*, 167–176. [CrossRef]
32. Ruben, R.B.; Fernandes, P.R.; Folgado, J. On the Optimal Shape of Hip Implants. *J. Biomech.* **2012**, *45*, 239–246. [CrossRef]
33. Tarlochan, F.; Mehboob, H.; Mehboob, A.; Chang, S.-H. Influence of Functionally Graded Pores on Bone Ingrowth in Cementless Hip Prosthesis: A Finite Element Study Using Mechano-Regulatory Algorithm. *Biomech. Model. Mechanobiol.* **2018**, *17*, 701–716. [CrossRef] [PubMed]

34. Ghosh, R.; Hazra, A.; Chanda, S.; Chakraborty, D. Computational Assessment of Growth of Connective Tissues around Textured Hip Stem Subjected to Daily Activities after THA. *Med. Biol. Eng. Comput.* **2023**, *61*, 525–540. [CrossRef] [PubMed]

35. Puthumanapully, P.K.; Browne, M. Tissue Differentiation around a Short Stemmed Metaphyseal Loading Implant Employing a Modified Mechanoregulatory Algorithm: A Finite Element Study. *J. Orthop. Res.* **2011**, *29*, 787–794. [CrossRef] [PubMed]

36. Ghosh, R.; Chanda, S.; Chakraborty, D. The Influence of Macro-Textural Designs over Implant Surface on Bone on-Growth: A Computational Mechanobiology Based Study. *Comput. Biol. Med.* **2020**, *124*, 103937. [CrossRef] [PubMed]

37. Mehboob, H.; Ahmad, F.; Tarlochan, F.; Mehboob, A.; Chang, S.H. A Comprehensive Analysis of Bio-Inspired Design of Femoral Stem on Primary and Secondary Stabilities Using Mechanoregulatory Algorithm. *Biomech. Model. Mechanobiol.* **2020**, *19*, 2213–2226. [CrossRef] [PubMed]

38. Moreo, P.; Pérez, M.A.; García-Aznar, J.M.; Doblaré, M. Modelling the Mechanical Behaviour of Living Bony Interfaces. *Comput. Methods Appl. Mech. Eng.* **2007**, *196*, 3300–3314. [CrossRef]

39. Ghosh, R.; Chanda, S.; Chakraborty, D. Influence of Sequential Opening/Closing of Interface Gaps and Texture Density on Bone Growth over Macro-Textured Implant Surfaces Using FE Based Mechanoregulatory Algorithm. *Comput. Methods Biomech. Biomed. Eng.* **2022**, *25*, 985–999. [CrossRef] [PubMed]

40. Büchler, P.; Pioletti, D.P.; Rakotomanana, L.R. Biphasic Constitutive Laws for Biological Interface Evolution. *Biomech. Model. Mechanobiol.* **2003**, *1*, 239–249. [CrossRef] [PubMed]

41. Tarala, M.; Janssen, D.; Verdonschot, N. Toward a Method to Simulate the Process of Bone Ingrowth in Cementless THA Using Finite Element Method. *Med. Eng. Phys.* **2013**, *35*, 543–548. [CrossRef]

42. Viceconti, M.; Ricci, S.; Pancanti, A.; Cappello, A. Numerical Model to Predict the Longterm Mechanical Stability of Cementless Orthopaedic Implants. *Med. Biol. Eng. Comput.* **2004**, *42*, 747–753. [CrossRef]

43. Prendergast, P. Finite Element Models in Tissue Mechanics and Orthopaedic Implant Design. *Clin. Biomech.* **1997**, *12*, 343–366. [CrossRef] [PubMed]

44. Ghosh, R.; Chanda, S.; Chakraborty, D. Application of Finite Element Analysis to Tissue Differentiation and Bone Remodelling Approaches and Their Use in Design Optimization of Orthopaedic Implants: A Review. *Int. J. Numer. Methods Biomed. Eng.* **2022**, *38*, e3637. [CrossRef] [PubMed]

45. Fröschen, F.S.; Wirtz, D.C.; Schildberg, F.A. Physiological reactions in the interface between cementless implants and bone. *Orthop. Heidelb. Ger.* **2023**, *52*, 178–185. [CrossRef] [PubMed]

46. Vio War, A.S.; Kumar, N.; Chanda, S. Does Preclinical Analysis Based on Static Loading Underestimate Post-Surgery Stem Micromotion in THA as Opposed to Dynamic Gait Loading? *Med. Biol. Eng. Comput.* **2023**, *61*, 1473–1488. [CrossRef] [PubMed]

47. Checa, S.; Prendergast, P.J. A Mechanobiological Model for Tissue Differentiation That Includes Angiogenesis: A Lattice-Based Modeling Approach. *Ann. Biomed. Eng.* **2009**, *37*, 129–145. [CrossRef] [PubMed]

48. Liu, X.; Niebur, G.L. Bone Ingrowth into a Porous Coated Implant Predicted by a Mechano-Regulatory Tissue Differentiation Algorithm. *Biomech. Model. Mechanobiol.* **2008**, *7*, 335–344. [CrossRef]

49. Buchanan, T.S.; Lloyd, D.G.; Manal, K.; Besier, T.F. Estimation of Muscle Forces and Joint Moments Using a Forward-Inverse Dynamics Model. *Med. Sci. Sports Exerc.* **2005**, *37*, 1911–1916. [CrossRef] [PubMed]

50. Lutz, A.; Nackenhorst, U. A Computational Approach on the Osseointegration of Bone Implants Based on a Bio-Active Interface Theory. *GAMM-Mitteilungen* **2009**, *32*, 178–192. [CrossRef]

51. Mathai, B.; Gupta, S. Bone Ingrowth Around an Uncemented Femoral Implant Using Mechanoregulatory Algorithm: A Multiscale Finite Element Analysis. *J. Biomech. Eng.* **2021**, *144*, 021004. [CrossRef]

52. Lutz, A.; Nackenhorst, U. Numerical Investigations on the Osseointegration of Uncemented Endoprostheses Based on Bio-Active Interface Theory. *Comput. Mech.* **2012**, *50*, 367–381. [CrossRef]

53. Taddei, F.; Pancanti, A.; Viceconti, M. An Improved Method for the Automatic Mapping of Computed Tomography Numbers onto Finite Element Models. *Med. Eng. Phys.* **2004**, *26*, 61–69. [CrossRef] [PubMed]

54. Viceconti, M.; Casali, M.; Massari, B.; Cristofolini, L.; Bassini, S.; Toni, A. The "standardized Femur Program" Proposal for a Reference Geometry to Be Used for the Creation of Finite Element Models of the Femur. *J. Biomech.* **1996**, *29*, 1241. [CrossRef] [PubMed]

55. Guedes, J.; Kikuchi, N. Preprocessing and Postprocessing for Materials Based on the Homogenization Method with Adaptive Finite Element Methods. *Comput. Methods Appl. Mech. Eng.* **1990**, *83*, 143–198. [CrossRef]

56. *Non-Homogeneous Media and Vibration Theory*; Lecture Notes in Physics; Springer: Berlin/Heidelberg, Germany, 1980; Volume 127, ISBN 978-3-540-10000-3.

57. Viceconti, M.; Muccini, R.; Bernakiewicz, M.; Baleani, M.; Cristofolini, L. Large-Sliding Contact Elements Accurately Predict Levels of Bone–Implant Micromotion Relevant to Osseointegration. *J. Biomech.* **2000**, *33*, 1611–1618. [CrossRef] [PubMed]

58. Oliveira, J.A.; Pinho-da-Cruz, J.; Teixeira-Dias, F. Asymptotic Homogenisation in Linear Elasticity. Part II: Finite Element Procedures and Multiscale Applications. *Comput. Mater. Sci.* **2009**, *45*, 1081–1096. [CrossRef]

59. Simões, J.A.; Marques, A.T. Design of a Composite Hip Femoral Prosthesis. *Mater. Des.* **2005**, *26*, 391–401. [CrossRef]

60. ISO 7206-8:1995. Available online: https://www.iso.org/standard/21009.html (accessed on 31 March 2024).

61. ISO 7206-4:2010. Available online: https://www.iso.org/standard/42769.html (accessed on 31 March 2024).

62. Bergmann, G.; Deuretzbacher, G.; Heller, M.; Graichen, F.; Rohlmann, A.; Strauss, J.; Duda, G.N. Hip Contact Forces and Gait Patterns from Routine Activities. *J. Biomech.* **2001**, *34*, 859–871. [CrossRef]

63. Heller, M.O.; Bergmann, G.; Kassi, J.-P.; Claes, L.; Haas, N.P.; Duda, G.N. Determination of Muscle Loading at the Hip Joint for Use in Pre-Clinical Testing. *J. Biomech.* **2005**, *38*, 1155–1163. [CrossRef] [PubMed]

64. Heller, M.O.; Bergmann, G.; Deuretzbacher, G.; Dürselen, L.; Pohl, M.; Claes, L.; Haas, N.P.; Duda, G.N. Musculo-Skeletal Loading Conditions at the Hip during Walking and Stair Climbing. *J. Biomech.* **2001**, *34*, 883–893. [CrossRef]

65. Pedersen, D.R.; Brand, R.A.; Davy, D.T. Pelvic Muscle and Acetabular Contact Forces during Gait. *J. Biomech.* **1997**, *30*, 959–965. [CrossRef]

66. Kuiper, J.H. Numerical Optimization of Artificial Hip Joint Designs. Ph.D. Thesis, Katholieke Universitcit Nijmegen, Nijmegen, The Netherlands, 1993.

67. Keaveny, T.M.; Bartel, D.L. Effects of Porous Coating, with and without Collar Support, on Early Relative Motion for a Cementless Hip Prosthesis. *J. Biomech.* **1993**, *26*, 1355–1368. [CrossRef] [PubMed]

68. Jasty, M.; Bragdon, C.; Burke, D.; O'Connor, D.; Lowenstein, J.; Harris, W.H. In Vivo Skeletal Responses to Porous-Surfaced Implants Subjected to Small Induced Motions. *J. Bone Joint Surg. Am.* **1997**, *79*, 707–714. [CrossRef] [PubMed]

69. Szmukler-Moncler, S.; Salama, H.; Reingewirtz, Y.; Dubruille, J.H. Timing of Loading and Effect of Micromotion on Bone-Dental Implant Interface: Review of Experimental Literature. *J. Biomed. Mater. Res.* **1998**, *43*, 192–203. [CrossRef]

70. Burke, D.W.; O'Connor, D.O.; Zalenski, E.B.; Jasty, M.; Harris, W.H. Micromotion of Cemented and Uncemented Femoral Components. *J. Bone Jt. Surg. Br.* **1991**, *73*, 33–37. [CrossRef] [PubMed]

71. Simmons, C.A.; Meguid, S.A.; Pilliar, R.M. Mechanical Regulation of Localized and Appositional Bone Formation around Bone-Interfacing Implants. *J. Biomed. Mater. Res.* **2001**, *55*, 63–71. [CrossRef]

72. Lutz, A.; Nackenhorst, U. Computation of Static-Equivalent Load Sets for Bone Remodeling Simulation. *PAMM* **2007**, *7*, 4020007–4020008. [CrossRef]

73. Huiskes, R.; Weinans, H.; Grootenboer, H.J.; Dalstra, M.; Fudala, B.; Slooff, T.J. Adaptive Bone-Remodeling Theory Applied to Prosthetic-Design Analysis. *J. Biomech.* **1987**, *20*, 1135–1150. [CrossRef] [PubMed]

74. Isaksson, H.; Wilson, W.; van Donkelaar, C.C.; Huiskes, R.; Ito, K. Comparison of Biophysical Stimuli for Mechano-Regulation of Tissue Differentiation during Fracture Healing. *J. Biomech.* **2006**, *39*, 1507–1516. [CrossRef] [PubMed]

75. Viceconti, M.; Monti, L.; Muccini, R.; Bernakiewicz, M.; Toni, A. Even a Thin Layer of Soft Tissue May Compromise the Primary Stability of Cementless Hip Stems. *Clin. Biomech. Bristol Avon* **2001**, *16*, 765–775. [CrossRef]

76. Lacroix, D.; Prendergast, P.J. A Mechano-Regulation Model for Tissue Differentiation during Fracture Healing: Analysis of Gap Size and Loading. *J. Biomech.* **2002**, *35*, 1163–1171. [CrossRef]

77. Carter, D.R.; Blenman, P.R.; Beaupré, G.S. Correlations between Mechanical Stress History and Tissue Differentiation in Initial Fracture Healing. *J. Orthop. Res. Off. Publ. Orthop. Res. Soc.* **1988**, *6*, 736–748. [CrossRef] [PubMed]

78. Lebon, F.; Ronel-Idrissi, S. Asymptotic Analysis of Mohr-Coulomb and Drucker-Prager Soft Thin Layers. *Steel Compos. Struct.* **2004**, *4*, 133–147. [CrossRef]

79. Robling, A.G.; Turner, C.H. Mechanical Signaling for Bone Modeling and Remodeling. *Crit. Rev. Eukaryot. Gene Expr.* **2009**, *19*, 319–338. [CrossRef] [PubMed]

80. Hadjidakis, D.J.; Androulakis, I.I. Bone Remodeling. *Ann. N. Y. Acad. Sci.* **2006**, *1092*, 385–396. [CrossRef] [PubMed]

81. Feyzi, M.; Fallahnezhad, K.; Taylor, M.; Hashemi, R. A Review on the Finite Element Simulation of Fretting Wear and Corrosion in the Taper Junction of Hip Replacement Implants. *Comput. Biol. Med.* **2021**, *130*, 104196. [CrossRef] [PubMed]

82. ASME. *V&V 40—2018: Assessing Credibility of Computational Modeling through Verification and Validation: Application to Medical Devices*; ASME: New York, NY, USA, 2018.

83. Santori, F.S.; Manili, M.; Fredella, N.; Tonci Ottieri, M.; Santori, N. Ultra-Short Stems with Proximal Load Transfer: Clinical and Radiographic Results at Five-Year Follow-Up. *Hip Int. J. Clin. Exp. Res. Hip Pathol. Ther.* **2006**, *16* (Suppl. S3), 31–39. [CrossRef]

84. Kohli, N.; Stoddart, J.C.; van Arkel, R.J. The Limit of Tolerable Micromotion for Implant Osseointegration: A Systematic Review. *Sci. Rep.* **2021**, *11*, 10797. [CrossRef]